Available online at www.sciencedirect.com
SCIENCE DIRECT®
ELSEVIER
International Journal of Multiphase Flow 31 (2005) 1181–1197
International Journal of Multiphase Flow
www.elsevier.com/locate/ijmulflow

Air transport in chute flows

Kristian Kramer [a,*], Willi H. Hager [b]

[a] *Lahmeyer International GmbH (LI), Bad Vilbel, Germany (formerly VAW)*
[b] *Laboratory of Hydraulics, Hydrology and Glaciology (VAW), Swiss Federal Institute of Technology, ETH, Zurich, Switzerland*

Received 5 August 2004; received in revised form 30 June 2005

Abstract

The air bubble rise velocity in still water depends mainly on the bubble size and is basically influenced by buoyancy, viscosity and surface tension. In high-speed flows the number of forces acting on air bubbles increases with turbulence, non-hydrostatic pressure gradient, shear forces, bubble clouds and free-surface entrainment. Air bubbles in these flows are used for cavitation protection of hydraulic structures such as chutes, spillways and bottom outlets. Here, air is normally added by means of aerators upstream of regions where the cavitation number falls below a critical value mainly to reduce the sonic velocity of the fluid and cushion the cavitation bubble collapse process. The distance between successive aerators depends basically on the bubble rise velocity. Until today, the bubble rise velocity in high-speed flows was not thoroughly investigated because of limited laboratory instrumentation. The present project focused on the streamwise development of air concentrations in high-speed flows along a 14 m long model chute. The bubble rise velocity was indirectly derived from the air detrainment gradient of the air concentration contour lines downstream of an aeration device. It accounts for the main hydraulic parameters chute slope, Froude number and air concentration. It is demonstrated that the bubble rise velocity in high-speed flow and stagnant water differ significantly due to fracturing processes, turbulence, and the ambient air concentration.

Keywords: Air bubble rise velocity; Cavitation protection; Chute flow; Fiber-optical instrumentation; High-speed flow; Turbulence; Two-phase flow

* Corresponding author.

0301-9322/$ - see front matter
doi:10.1016/j.ijmultiphaseflow.2005.06.006

1. Introduction

A key problem of high-velocity open channel or chute flows is the potential of cavitation damage along the chute bottom and side walls. Air added to high-speed water flows is known to reduce the sonic fluid velocity and thus the risk of cavitation damage, such that chute inverts are protected by sufficient air presence close to the chute boundaries with so-called chute aerators. They are placed in regions where the cavitation number is small, where natural free-surface aeration has not yet reached the chute floor, or where the air added has detrained. The distance required between two aerators for optimum chute protection is not yet established because the air detrainment process is currently not fully understood (Falvey, 1980, 1990; Chanson, 1989, 1997; Kramer et al., 2002). Fig. 1 shows a typical photograph of the air bubble distribution in such two-phase flows with large air concentration and bubble size close to the free surface.

Currently no reliable design guidelines exist for the distance required between two aerators, although aerators have been proposed as early as in the 1970s. Whereas the motion of air bubbles in still water were investigated e.g. by Haberman and Morton (1956), there is presently a gap of knowledge on the behaviour of air bubbles in high-speed flows. The forces acting on air bubbles in chute flows are more complicated as those in still water. Furthermore, no detailed laboratory experiments were conducted because of limited laboratory instrumentation. Because optical systems fail in turbulent flows with a large air concentration, modern fiber-optical systems were used

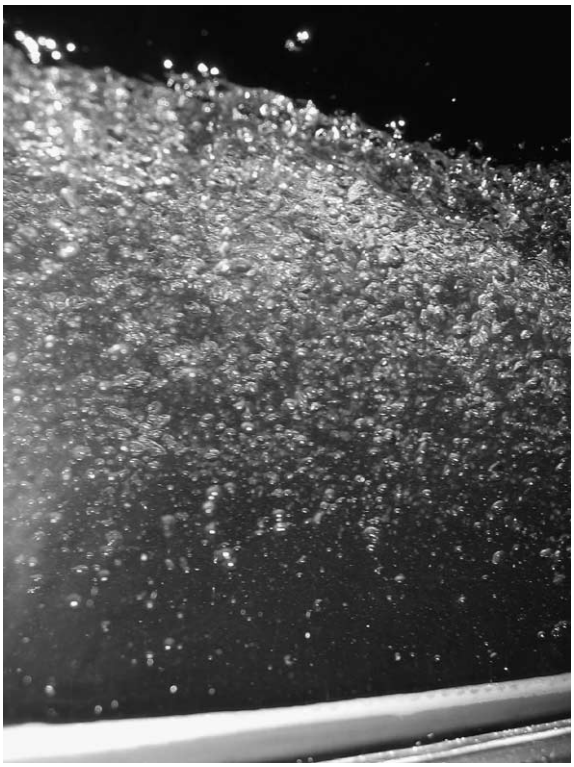

Fig. 1. Typical air bubble distribution in high-speed flow, flow from left to right (Möller, 2003).

herein to detect bubbles and droplets. This paper presents air concentration measurements in chute flows using fiber-optical instrumentation and describes the time-averaged behaviour of air–water two-phase flows.

2. Air bubble rise velocity

2.1. Transport principle

According to Falvey and Ervine (1988), the transport of a single bubble is mainly influenced by four forces, namely: (1) inertia, (2) drag, (3) buoyancy, and (4) turbulent eddy transport. Rutschmann et al. (1986) found in addition an effect of the non-hydrostatic pressure gradient on the bubble rise velocity, and Kobus (1991) mentioned an influence of bubble clouds on the single bubble transport process. Fig. 2 shows schematically the various forces acting on air bubbles in chute flow.

The bubble transport process was developed in fluid mechanics, heat transfer, biochemistry and nuclear engineering (Soo, 1967; Braeske et al., 1997). A basic contribution on the rise velocity of a single bubble in still water is due to Haberman and Morton (1956) (Fig. 3). The Stokes' law of drag on rigid spherical bubbles was improved. Comolet (1979) based his findings on Haberman and Morton's and his own experimental tests and provided a theory based on the drag, the weight, and the buoyant forces. The motion of a single bubble is often expressed in dimensional terms with the bubble (subscript bu) rise velocity u_{bu} versus the equivalent bubble diameter d_{bu}. The drag resistance coefficient was also related to the bubble Reynolds number $\mathbf{R}_{bu} = u_{bu}d_{bu}/v$, with v as the kinematic viscosity of water.

2.2. Governing equations

Expressions of the dimensional rise velocity are plotted in Fig. 3. The transport of small rigid spherical bubble depends on surface tension. With g as gravitational acceleration, ρ_a density of

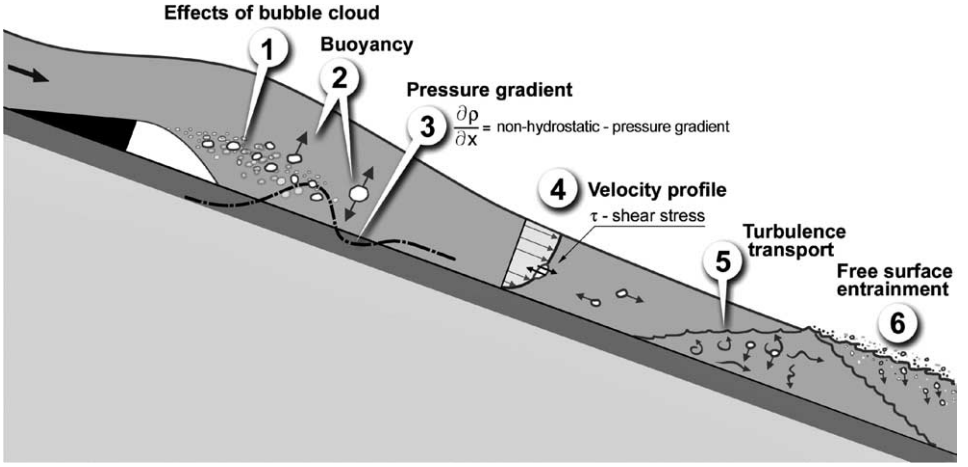

Fig. 2. Forces acting on air bubbles downstream of a chute aerator.

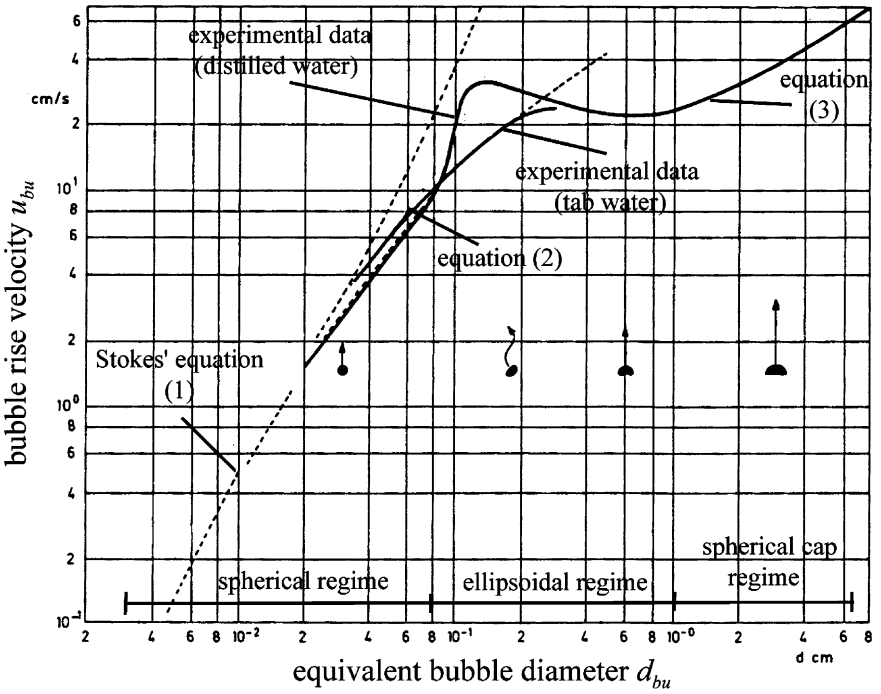

Fig. 3. Bubble rise velocity in still water as a function of bubble size (Haberman and Morton, 1956).

air, and ρ_w density of water, air bubbles in water with $d_{bu} < 0.068$ mm follow according to Stokes (Falvey, 1980)

$$u_{bu} = \frac{2}{9}\frac{d_{bu}^2 g}{\nu}\left(1 - \frac{\rho_a}{\rho_w}\right). \tag{1}$$

For air bubbles with $0.068\text{ mm} < d_{bu} < 0.80$ mm, the bubble rise velocity is (Comolet, 1979)

$$u_{bu} = \frac{1}{18}\frac{d_{bu}^2 g}{\nu}\left(1 - \frac{\rho_a}{\rho_w}\right). \tag{2}$$

With increasing bubble size, the bubble shape changes from spherical to oblate spheroid with the bubbles rising along an irregular or spiral trajectory (Kobus, 1991). Comolet (1979) observed that both surface tension and buoyancy are important, and suggested for bubbles with $0.80\text{ mm} < d_{bu} < 10$ mm

$$u_{bu} = \sqrt{0.52 g d_{bu} + 2.14\frac{\sigma_t}{\rho_w d_{bu}}}, \tag{3}$$

with σ_t as the interfacial surface tension between air and water. For bubbles exceeding $d_{bu} = 10$ mm surface tension effects can be neglected and the rise velocity follows simply (Falvey, 1980)

$$u_{bu} = \sqrt{g d_{bu}}. \tag{4}$$

2.3. Air bubbles in high-speed flow

2.3.1. Turbulence

Turbulence reduces the terminal bubble rise velocity, because turbulent shear fractures larger bubbles into smaller bubbles. Falvey (1980) estimated the critical bubble size $d_{bu(95)}$ from the loss of energy according to Hinze (1975). He therefore proposed an equation of Rouse (1950) to account for the energy loss by the energy slope S_E for the critical bubble size as

$$d_{bu(95)} = 0.725\left[\left(\frac{\sigma_t}{\rho_w}\right)^3\left(\frac{1}{gS_E\bar{u}}\right)^2\right]^{\frac{1}{5}}. \tag{5}$$

Here $d_{bu(95)}$ is the bubble diameter for which less than 95% of the air is contained in this bubble diameter, and $\bar{u}$ is the average flow velocity. If u_{bu} is the terminal bubble rise velocity in still water, then u_{but} is the terminal rise velocity in turbulent flow. Expressing $u_{but} = a \cdot u_{bu}$ with a as a coefficient versus the dimensionless discharge $Q_w^2/(gh_w^5)$, where Q_w is water discharge and h_w the flow depth, only rising bubbles may be considered with this relation. For $Q_w^2/(gh_w^5) > 5$, the empirical coefficient is $a \approx 0.25$; air bubbles then rise four times slower than in still water. Chanson and Toombes (2002) supported this approach. The presence of finer bubbles was attributed to bubble break-up processes by turbulent shear.

2.3.2. Bubble clouds

A bubble cloud in stagnant water moves with a considerably larger mean velocity than a single bubble because of the upward current. This effect is counteracted in the same order of magnitude by bubbles being displaced laterally along their paths and a less induced vertical water flow (Kobus, 1991). Volkart (1985) explained the reduced bubble rise velocity in his laboratory investigations by the large number of bubbles in mutual contact and interference, resulting in collisions, deformations, bubble collapse and bubble coalescence, and thus a loss of kinetic energy and higher drag of air bubbles.

2.3.3. Non-hydrostatic pressure

According to Rutschmann et al. (1986) the bubble rise velocity in the impact zone of jets onto a chute bottom is affected by a non-hydrostatic pressure gradient. The effect of the vertical pressure gradient dp/dz on the bubble rise velocity results from the balance between the upward turbulent diffusion and the downward pressure gradient. Although their equation proposed was dimensionally incorrect the effect of non-hydrostatic pressure gradient on the bubble rise velocity is retained.

Wood (1988) predicted the bubble rise velocity in non-hydrostatic pressure conditions similarly. Using the results of Rutschmann et al. (1986) and Chanson (1988) he found that pressure at the impact zone may become much larger than the hydrostatic pressure. This over-pressure leads to pressure gradients resulting in massive air detrainment in the impact region. According to Chanson (1988) the non-hydrostatic pressure gradient is responsible for the bubble rise velocity, i.e.

$$u_{but}^2 = u_{bu}^2 \frac{1}{\rho_w g}\frac{dp}{dz}, \tag{6}$$

where u_{bu} is the bubble rise velocity in stagnant water from (1)–(4). The bubble transport direction depends on the algebraic sign of the pressure gradient; bubbles thus rise towards the free surface for $dp/dz > 0$, whereas they are captured by the flow if $dp/dz < 0$. Fig. 2 shows air bubbles downstream of an aerator subjected to these effects. According to Volkart (1985) the bubble rise velocity in turbulent flow may be 10 times slower than in still water, i.e.

$$u_{but} = u_{bu}/10. \tag{7}$$

3. Experiments

3.1. Hydraulic chute

A 14 m long prismatic rectangular chute model of $b = 0.50$ m wide was used for the two-phase flow investigations with a variable bottom slope $0\% \leqslant S_o \leqslant 50\%$, a variable inflow depth up to $h_o = 0.12$ m and discharges up to $Q_w = 250$ l/s (Fig. 4). The automatically driven measuring system carried a fiber-optical probe manufactured by *RBI*, Grenoble, France. The large data sets were collected and analysed automatically with a graphical user interface based on *Matlab*. Preliminary investigations were conducted to verify the experimental accuracy (Kramer, 2004). All quantities, namely: (1) water discharge Q_w, (2) air discharge Q_a, (3) positioning in the streamwise x- and the perpendicular to the chute bottom z directions, and (4) automised data collection were controlled by an in-house designed *LabView* program. Automatic data acquisition including air concentration profiles, and bubble size distribution were also sampled by programs based on *Matlab*.

Fig. 4. Photograph of VAW chute model.

Two distinctly different air supply devices to generate air-water flow were employed: (1) deflector similar to a prototype aerator, and (2) pre-aerated flow by adding air to the supply pipe. These allowed to analyse the effect of the approach flow conditions on the development of the air transport along the chute model. Both set-ups were investigated separately to determine their effects of the remaining hydraulic parameters. This paper focuses on the pre-aerated data sets. Differences between the two air supply systems were presented by Kramer (2004).

3.2. Measuring system

A fiber-optical probe measured the following quantities: (1) local air concentration C, (2) mixture flow velocity u_m, and (3) bubble diameter d_{bu}, besides other statistical parameters. The basic principle of the fiber-optical instrumentation was described by Boes (2000). Measured data were time-averaged over usually 20 s. No air concentration can be deduced with this technique for $C < 0.0001$, a value irrelevant for chute flow. Measurement spacing was set inversely proportional to the gradients dC/dx and dC/dz, i.e. a variable grid system was defined to collect more information at reaches with large concentration gradients. Compared to Boes (2000) a new software detected 200,000 instead of 4000 signals (air bubbles) with a scan rate of 2000 Hz, along with a reduced computational time to handle the large data sets. Therefore, the measurement was intercepted after 20 s even for a high bubble frequency. A complete set of data involved more than 664 data points for each run in a test series.

Various attempts were made to determine the turbulence intensity from the RBI instrumentation, such as estimating the Reynolds turbulence term by substituting instantaneous velocity with the average mixture flow velocity u_m plus a fluctuation term v'_a. For the latter an instantaneous bubble velocity v'_a was separated from the mean mixture velocity, assuming that bubble size remains constant, i.e. $u = u_m + v'_a$. The attempt failed because of the temporally variable bubble size. The turbulent boundary layer was finally calculated by standard equations (e.g. Schlichting and Gersten, 1996). A detailed description of the measuring system and the chute model is given by Kramer (2004).

3.3. Air concentration contours and gradients

Local air concentration, flow velocity and air bubble size were determined by interpolated contour lines and air concentration profiles. The mixture flow depth h_{90} and the average air concentration $\overline{C}_{90}$ were defined in terms of the standard air concentration $C = 90\%$. A non-dimensional coordinate system $X_{90u} = x/h_{90u}$ and $Z_{90u} = z/h_{90u}$ was adopted, with the uniform (subscript u) mixture flow depth h_{90u} measured at the chute end. Fig. 5 shows air concentration contours for a horizontal chute in which the inflow Froude number $\mathbf{F}_o = (Q_w + Q_a)/(gh_o^3b^2)^{1/2}$, the inflow depth h_o and the surface roughness were kept constant. The local air bubble rise velocity was indirectly determined using the gradient $dZ(C)/dX(C)$, thereby assuming that air bubbles do not rise with a steady velocity u_{bu} but depend on local air concentration and turbulence. The contour lines considered for the analysis involved air concentrations of $C = 5.0\%$, $C = 1.0\%$ and $C = 0.1\%$, respectively. They rise steadily along the chute model until levelling-off at a point determined individually for each run. The detrainment gradient

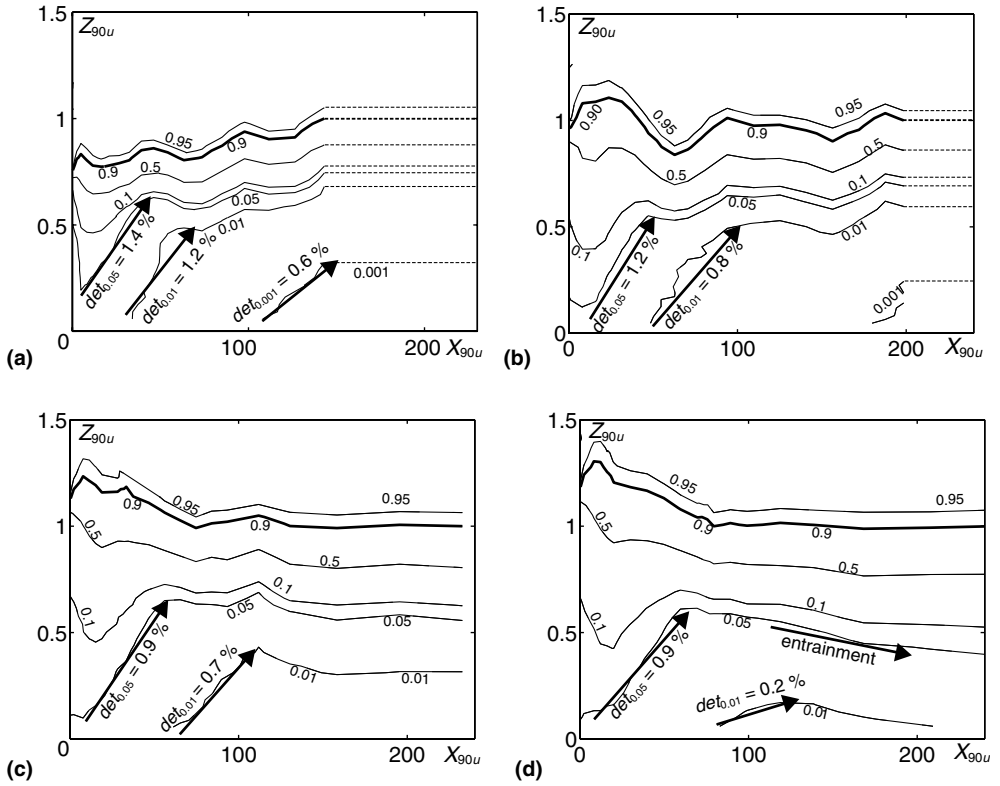

Fig. 5. Air concentration contour plots for $\mathbf{F}_o = 10.3$, $h_o = 0.06$ m, $\beta = Q_a/Q_w = 0.21$, (a) $S_o = 0\%$, $h_{90u} = 0.087$ m, (b) $S_o = 10\%$, $h_{90u} = 0.064$ m, (c) $S_o = 30\%$, $h_{90u} = 0.054$ m, and (d) and $S_o = 50\%$, $h_{90u} = 0.051$ m.

$$det_{(C)} = \frac{dZ_{90u}(C)}{dX_{90u}(C)} = \frac{\frac{\partial C}{\partial X_{90u}}}{\frac{\partial C}{\partial Z_{90u}}} \tag{8}$$

was defined between the lower starting point of the contour line and the kink with respect to the selected air concentration. Small air concentrations $C = 1.0\%$ and $C = 0.1\%$ were correlated with small bubble rise velocities or detrainment gradients, therefore. Downstream from the kink the contour lines either remain parallel to the chute bottom or decrease almost linearly. The 5.0% contour line seems to be unaffected by the bottom slope whereas the contour $det_{0.01}$ flattens for steeper chutes. For the inflow Froude number $\mathbf{F}_o = 10.3$ the air concentration falls below $C = 0.1\%$ only at the chute end (Fig. 5). Tests with other $\mathbf{F}_o$ were discussed by Kramer (2003).

3.4. Bubble size distribution

The bubble size d_{bu} [mm] is of major importance for the bubble rise velocity (Fig. 3). The fiber-optical measuring system detected the local bubble sauter cord size by means of flow velocity, frequency and time-averaged air concentration using a statistic algorithm. It relies on all three parameters, except in flow regions where bubbles remained undetected. Fig. 6(a) shows the bubble

size distribution d_{bu} [mm] over the non-dimensional chute length X_{90u} and the flow depth Z_{90u} using contour plots. The bold line represents the mixture flow depth h_{90}. In the lower flow zone $0 \leqslant Z_{90u} \leqslant 0.2$, the bubble size is small with $d_{bu} < 1.0$ mm due to high turbulence. The zone $0.2 \leqslant Z_{90u} \leqslant 0.7$ is represented by bubble diameters $1.0\text{ mm} \leqslant d_{bu} \leqslant 5.0$ mm, similar to the size

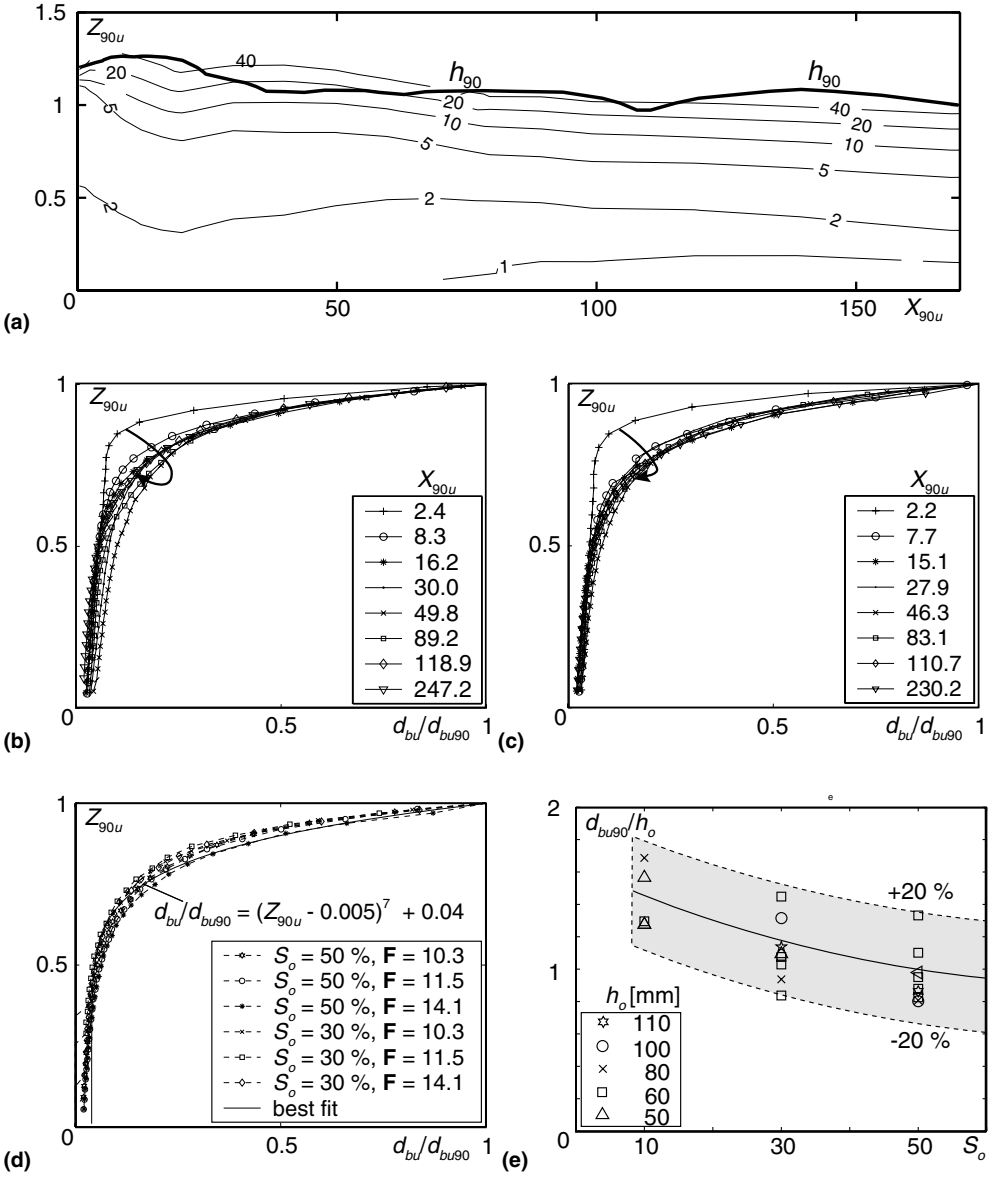

Fig. 6. Bubble size distribution for $h_o = 0.06$ m, $\beta = Q_a/Q_w = 0.21$, $S_o = 50\%$, (a) contour lines $d_{bu}(Z_{90u})$ [mm] $\mathbf{F}_o = 10.3$, $h_{90u} = 0.051$ m, (b) bubble size profiles d_{bu}/d_{bu90} against Z_{90u} for $\mathbf{F}_o = 10.3$, $h_{90u} = 0.051$ m, (c) $\mathbf{F}_o = 14.1$, $h_{90u} = 0.054$ m, and (d) typical uniform profiles, (—) best fit, (e) bubble size in the top region d_{bu90} divided by the inflow depth h_o versus chute slope S_o for various measurements.

quoted by, e.g. Haberman and Morton (1956). For $Z_{90u} \geqslant 0.7$ air bubbles increase rapidly due to air pockets ejected from the flow into the atmosphere. This finding is supported by Fig. 6(b) and (c), showing bubble size profiles d_{bu}/d_{bu90} against Z_{90u} for selected locations X_{90u} along the chute. The first profile of Fig. 6(b) at $X_{90u} = 2.4$ ($x = 0.122$ m) was influenced by the jetbox. All profiles further downstream increase up to $X_{90u} = 49.8$ ($x = 2.540$ m) before decreasing to uniform conditions. Fig. 6(c) shows a similar trend for a higher approach Froude number; larger turbulence accelerates the bubble development such that uniform bubble distribution is attained earlier. Measurements of the uniform flow region suggest for the characteristic bubble size distribution (Fig. 6(d))

$$d_{bu}/d_{bu90u} = (Z_{90u} - 0.005)^7 + 0.04 \quad S_o \geqslant 30\%. \tag{9}$$

The bubble size in the uniform region d_{bu90u} divided by the inflow depth h_o against the chute slope S_o is shown in Fig. 6(e). The bubble size is of the order of the inflow depth $0.8 \leqslant d_{bu90u}/h_o \leqslant 1.6$, with a decreasing trend for steeper chute slopes. This demonstrates that air pockets instead of air bubbles represent the mixing region with an air concentration of $C = 90\%$, as described, e.g. by Falvey (1980). Fig. 6 demonstrates, at least qualitatively, that a constant bubble size distribution in chute flow is unrealistic in highly turbulent flows. Assuming a constant bubble rise velocity as proposed in the literature seems to be questionable when considering u_{bu} as a function of the bubble size.

4. Development of air concentration isolines

4.1. Effect of Froude number

The increase of the air concentration isoline is defined by Eq. (8), and typical examples are shown in Fig. 5. Individual detrainment gradients were taken for all measurements (Kramer, 2004). Air detrainment gradients $det_{(C)}$ are influenced by the local air concentration C and the local air bubble rise velocity u_{bu}. Rise velocities are low in regions of small air bubbles $d_{bu} \leqslant 2$ mm (Fig. 6). In the following, the effect of the inflow Froude number $\mathbf{F}_o$ on the air detrainment gradients $det_{(C)}$ is analysed.

Fig. 7 shows air detrainment gradients $det_{(C)}$ against $\mathbf{F}_o$ for the four chute slopes investigated relative to $C = 5.0\%$, 1.0% and 0.1%. The linear trend lines correlate with the gradients $det_{(0.05)}$, $det_{(0.01)}$ and $det_{(0.001)}$. The trend of $det_{(0.05)}$ is relatively weak, although a larger air concentration seems to give smaller gradients for high Froude numbers, whereas the detrainment is larger for smaller Froude numbers. Despite the data scatter a relation between the inflow Froude number $\mathbf{F}_o$ and the air detrainment gradient $det_{(C)}$ was established for the $C = 1.0\%$ and the $C = 0.1\%$ contour lines. The $det_{(0.001)}$ trend line is below $det_{(0.01)}$, indicating that a small air presence remains longer in chute flow.

For gradients $det_{(0.01)}$ and $det_{(0.001)}$ equal to zero, the air concentration $C = 1.0\%$ or $C = 0.1\%$ never fell below these values along the entire chute. The air concentration thus had a minimum of $C = 0.1\%$ for $\mathbf{F}_o \geqslant 14.5$ in the horizontal chute (Fig. 7(a)) and $\mathbf{F}_o \geqslant 8.3$ for $S_o = 50\%$ (Fig. 7(d)). Likewise, the air concentration always fell below $C = 1\%$ in horizontal chutes but never below this value for $\mathbf{F}_o \geqslant 10.7$ and $S_o = 50\%$. Measurements for chute slopes $10\% \leqslant S_o \leqslant 30\%$ are inter-

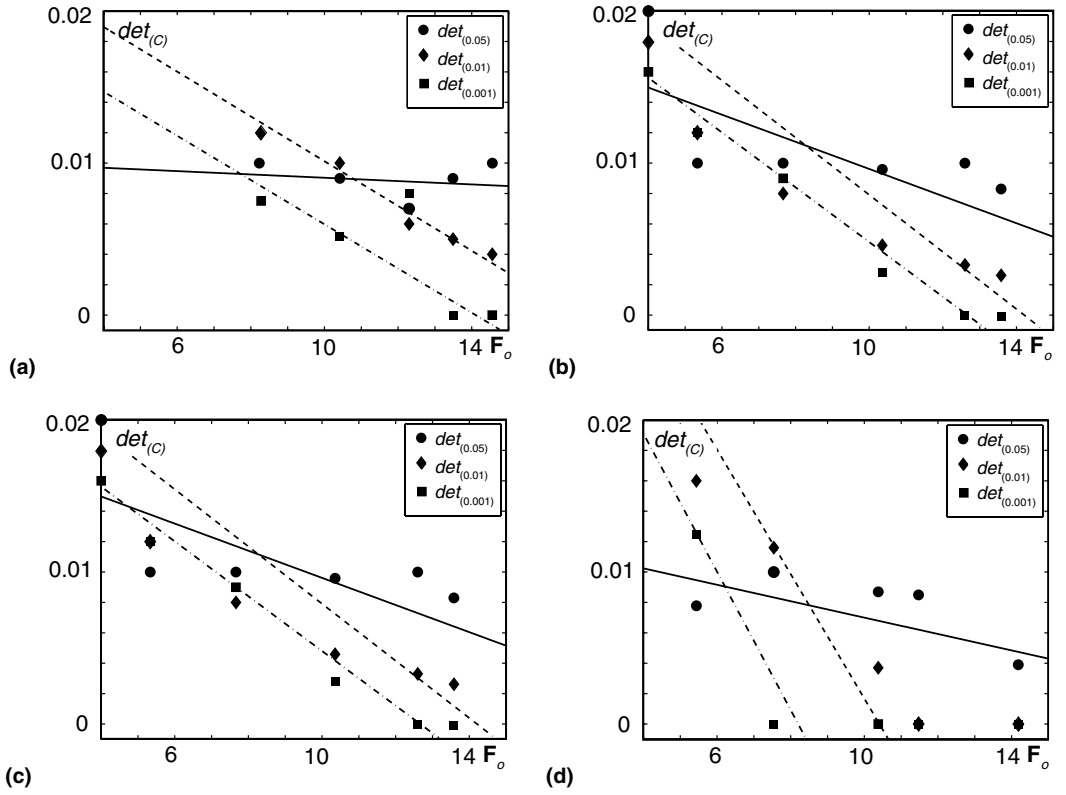

Fig. 7. Air detrainment gradient as a function of inflow Froude number $\mathbf{F}_o$ with linear trend lines $det_{(0.05)}$ (—), $det_{(0.01)}$ (- - -) and $det_{(0.001)}$ (-·-·-), for (a) $S_o = 0\%$, (b) $S_o = 10\%$, (c) $S_o = 30\%$, and (d) $S_o = 50\%$.

mediate to the extremes investigated. Therefore, both Froude number *and* chute slope influence the air detrainment gradients.

4.2. Effect of chute slope

Fig. 8 shows trend lines for $C = 1.0\%$ and $C = 0.1\%$; those for $det_{(0.05)}$ were dropped because of large data scatter and the irrelevance in engineering practice. The trend line for the horizontal chute $S_o = 0\%$ (—) is at the top with the largest detrainment gradients for $det_{(0.01)}$ and $det_{(0.001)}$, respectively. For larger chute slopes the trend lines steepen, indicating smaller air detrainment gradients for a given $\mathbf{F}_o$. The gradient $det_{(C)}$ is thus a function of air concentration, inflow Froude number and chute slope

$$det_{(C)} = -a\mathbf{F}_o + b, \tag{10}$$

with $a = f(S_o)$. The common point $b = a\mathbf{F}_b + det_b$ depends on the air concentration C, where $\mathbf{F}_{b(C)}$ is the inflow Froude number $\mathbf{F}_o$ at point b and $det_{b(C)}$ is the corresponding detrainment gradient $det_{(C)}$. The data may be expressed with the two parameters $det_{b(0.01)} = 0.015$ and $\mathbf{F}_{b(0.01)} = 6.9$ for $C = 1.0\%$, and $det_{b(0.001)} = 0.012$ and $\mathbf{F}_{b(0.001)} = 5.8$ for $C = 0.1\%$ as

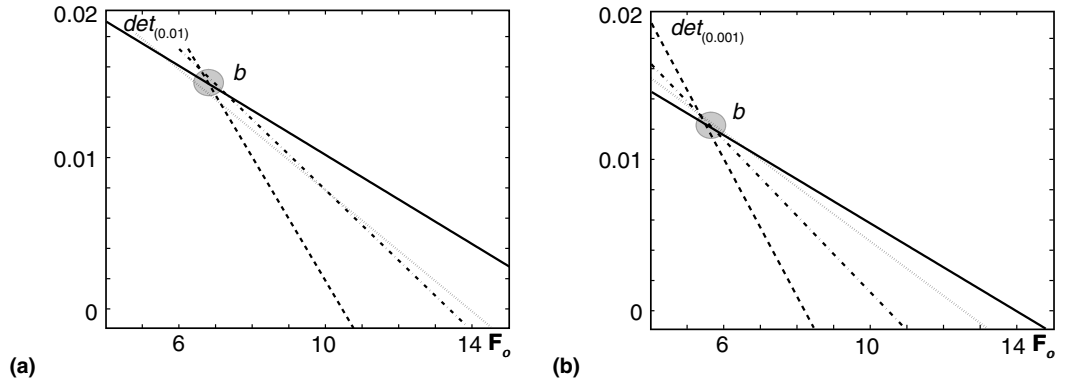

Fig. 8. Air detrainment gradients $det_{(C)}$ as a function of inflow Froude number $\mathbf{F}_o$ for $S_o = 0.0\%$ (—), $S_o = 10\%$ (···), $S_o = 30\%$ (-·-·-·), $S_o = 50\%$ (---), (a) $det_{(0.01)}$, and (b) $det_{(0.001)}$.

$$det_{(C)} = -a(\mathbf{F}_o - \mathbf{F}_{b(C)}) + det_{b(C)}. \tag{11}$$

The variable a as shown in Fig. 9(a) for the four chute slopes and for $det_{(0.01)}$ and $det_{(0.001)}$ is almost independent of air concentration. The air concentration influences the location of point b in Fig. 8, but the slope a is a function of chute slope only. The best fit for a is (Fig. 9(a))

$$a = 1.4 \times 10^{-3}[1 + 0.5\tan(2.7\sin\alpha)] \quad 0 \leqslant \sin\alpha \leqslant 0.5. \tag{12}$$

Combining (11) and (12) yields with the previously set constants $det_{b(C)}$ and $\mathbf{F}_{b(C)}$ (Kramer, 2004)

$$det_{(C)} = -1.4 \times 10^{-3}[1 + 0.5\tan(2.7\sin\alpha)] \cdot (\mathbf{F}_o - \mathbf{F}_{b(C)}) + det_{b(C)} \quad 0 \leqslant \sin\alpha \leqslant 0.5. \tag{13}$$

Eq. (13) is based on a large number of test conditions in the turbulent smooth regime. It may serve for the estimation of the flow features in prototype chutes where experimentation is difficult.

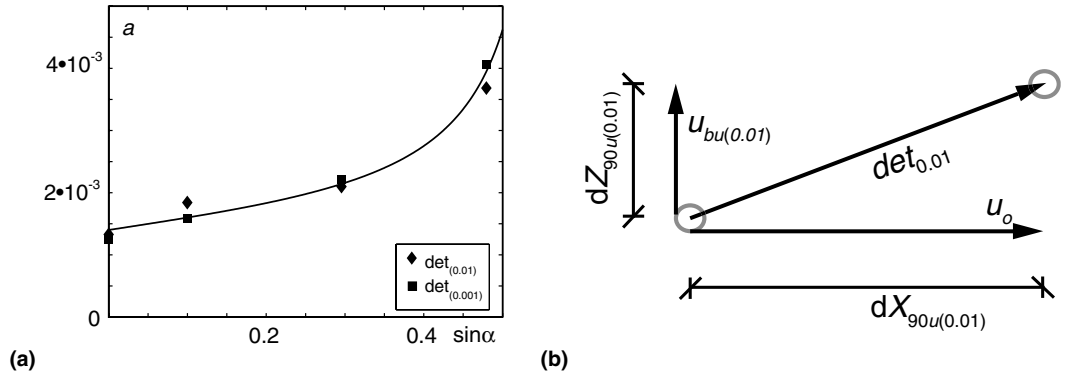

Fig. 9. (a) Variable a as a function of chute angle α with (—) Eq. (12), and (b) definition sketch for bubble rise velocity $u_{bu(C)}$ depending on average flow velocity u_o and air detrainment gradient $det_{(C)}$.

5. Bubble rise velocity

The fiber-optical probe is a 1D measuring system, allowing for a direct link between air concentration and bubble rise velocity u_{bu}. Although bubble size d_{bu} was determined, a relation between the bubble size d_{bu} and the bubble rise velocity u_{bu} seems to be uncertain in highly turbulent flow. Moreover, the bubble size varies with turbulence and air concentration, as discussed. Accordingly, a novel approach between the air concentration C and the bubble rise velocity u_{bu} was sought. It was determined using the air detrainment gradient $det_{(C)}$ according to (8) describing the increase of air concentration contours with distance, thereby accounting indirectly for the average inflow velocity $u_o = (Q_w + Q_a)/(bh_o)$. The time-averaged bubble rise velocity with respect to the air concentration C was thus defined as

$$u_{bu(C)} = det_{(C)} u_o. \tag{14}$$

The air concentration contour lines $C = 1.0\%$ and $C = 0.1\%$ referring to $det_{(0.01)}$ and $det_{(0.001)}$ were used to determine the bubble rise velocity $u_{bu(0.01)}$ and $u_{bu(0.001)}$, where $u_{bu(0.01)}$ refers to the rise velocity for the $C = 1\%$ air concentration contour line, as shown in Fig. 9(b). For a detrainment gradient $det_{(0.01)} = dZ_{90u}/dX_{90u} = 0.32/40 = 0.008$ relating to the $C = 1\%$ contour and an average inflow velocity of $u_o = 9$ m/s the bubble rise velocity is $u_{bu(0.01)} = det_{(0.01)} u_o = 0.008 \cdot 9 = 0.072$ m/s or 7.2 cm/s. Chanson (1989) considered a constant bubble rise velocity for air detrainment processes, namely $u_{bu} = 0.16$ m/s for scale models, and $u_{bu} = 0.40$ m/s for prototypes. However, Fig. 7 shows that the air concentration contours related to small air concentrations decay slower than those relating to larger air concentrations. This can be explained either by: (1) small air concentration contours refer to small air bubbles whose rise velocity is reduced according to Fig. 3, or (2) turbulent and diffusive effects act as a random generator and distribute air bubbles in regions with smaller air concentrations. This section presents bubble rise velocities using (14). Fig. 10 shows non-dimensional bubble rise velocity

$$\mathbf{U}_{bu} = \frac{u_{bu(C)}}{\sqrt{g h_o}}, \tag{15}$$

related to $C = 1.0\%$ as a function of the streamwise average Froude number

$$\mathbf{F}_{o-P} = \frac{\mathbf{F}_o + \mathbf{F}_P}{2}, \tag{16}$$

using the arithmetic average of Froude numbers at the inflow $\mathbf{F}_o$ and at the kink of the contour line $\mathbf{F}_P$. It incorporates thus the average flow behaviour in the region where the air bubbles actually rise, and furthermore includes the drawdown effect and thus indirectly the increase of turbulence and shear. The data of Fig. 10 refer to the four investigated chute slopes. Despite the data scatter, $\mathbf{U}_{bu}$ reduces as $\mathbf{F}_{o-P}$ increases. Further, the bubble rise velocity falls to zero for $\mathbf{F}_{o-P} \geqslant 13.8$, indicating that air bubbles associated with $C = 1\%$ are then kept at the chute bottom. With $\mathbf{F}_0$ as the Froude number where $\mathbf{U}_{bu} = 0$, a constant slope $t = 0.029$ for $\mathbf{F}_0 = 13.7$ and $C = 1\%$ was obtained in (Fig. 10)

$$\mathbf{U}_{bu} = -t(\mathbf{F}_{o-P} - \mathbf{F}_0) \quad \mathbf{F}_{o-P} \geqslant 7.5. \tag{17}$$

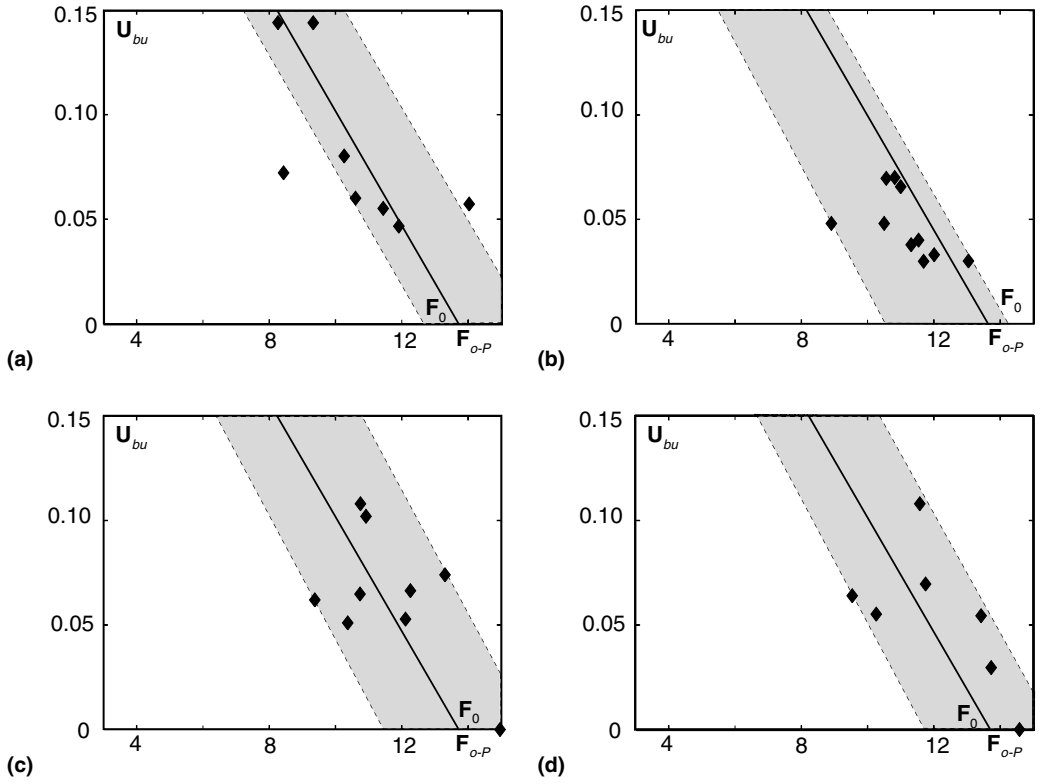

Fig. 10. Non-dimensional bubble rise velocity $\mathbf{U}_{bu}$ for $C = 1.0\%$ as a function of streamwise Froude number $\mathbf{F}_{o-P}$, (—) trend line with $t = 0.029$ from (17) for (a) $S_o = 0\%$, (b) $S_o = 10\%$, (c) $S_o = 30\%$, and (d) $S_o = 50\%$.

Eq. (17) is limited to $\mathbf{F}_{o-P} \geqslant 7.5$ and $\mathbf{U}_{bu} \leqslant 0.15$ for $C = 1.0\%$, and to $\mathbf{U}_{bu} \leqslant 0.10$ for $C = 0.1\%$ (Fig. 11). These were the maximum non-dimensional bubble rise velocities observed. From a physical point of view, the non-dimensional bubble rise velocity reduces for steeper chute slopes due to increasing turbulence. It is therefore evident that slopes of the trend lines t in Fig. 10 increase for steeper chutes. They are constant because the streamwise Froude number $\mathbf{F}_{o-P}$ accounts for the effect of slope. The parameter $\mathbf{F}_{o-P}$ incorporates the gross flow features with a reducing flow depth $h(x)$ in the tailwater direction. Note that this analysis is a simple approach for the bubble rise velocity in turbulent flow. Fig. 11 refers to the $C = 0.1\%$ air concentration, from which a similar trend as in Fig. 10 may be noted. The slope of the trend line was also $t = 0.029$ but they intersect the x-axis at $\mathbf{F}_0 = 11.8$; the bubble rise velocity is thus zero for a higher streamwise Froude number.

The non-dimensional bubble rise velocity $\mathbf{U}_{bu}$ depends exclusively on the streamwise Froude number $\mathbf{F}_{o-P}$. Fig. 12 shows a summary plot of all dimensional bubble rise velocities u_{bu} in [m/s] according to Eq. (14) for all investigated chute slopes against the inflow Froude number $\mathbf{F}_o$ for the range of u_{bu}considered in this project. Typically, one has $0.02\ \text{m/s} \leqslant u_{bu} \leqslant 0.12\ \text{m/s}$ in Fig. 12(a), and $0.0 \leqslant u_{bu} \leqslant 0.08$ m/s in Fig. 12(b). The bubble rise velocity in model chute flow

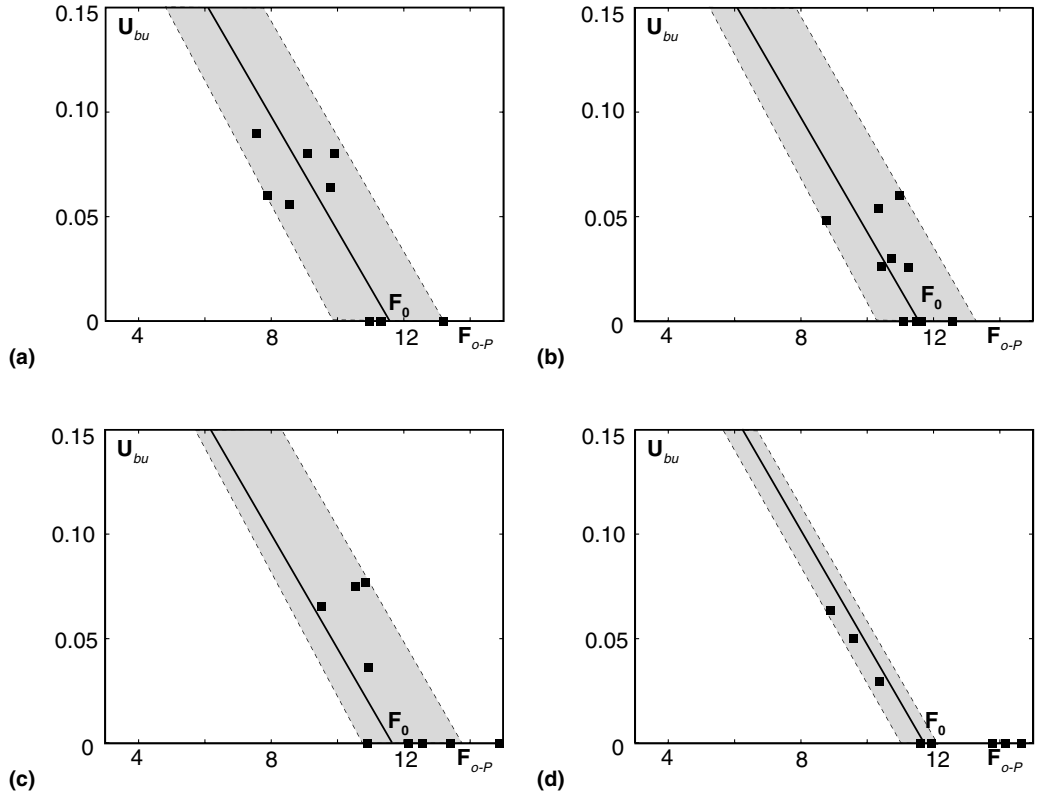

Fig. 11. Non-dimensional bubble rise velocity $\mathbf{U}_{\mathrm{bu}}$ (15) for $C = 0.1\%$ as a function of streamwise Froude number $\mathbf{F}_{o-P}$ (16), (—) trend line with $t = 0.029$ (17) for (a) $S_{\mathrm{o}} = 0\%$, (b) $S_{\mathrm{o}} = 10\%$, (c) $S_{\mathrm{o}} = 30\%$, and (d) $S_{\mathrm{o}} = 50\%$.

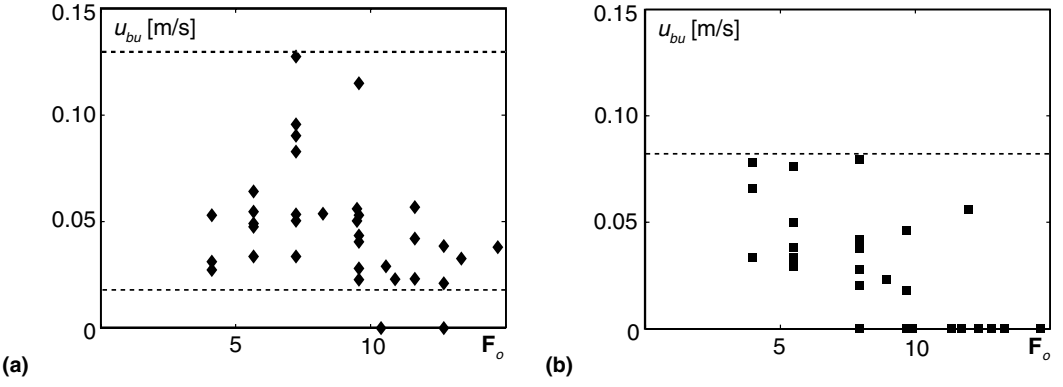

Fig. 12. Dimensional bubble rise velocity u_{bu} [m/s] against inflow air concentration $\mathbf{F}_o$ (a) $C = 1.0\%$, and (b) $C = 0.1\%$.

using a Froude model is of the order $u_{\mathrm{bu}} \approx 0.08$ m/s for the investigated air concentrations, therefore.

6. Conclusions

This project presents systematic measurements of air concentration profiles in high-speed chute flow along with information on the streamwise air concentration, flow velocity and bubble size for a large number of data. A complete automation of both the measuring probe and the data analysis was necessary to cover a wide range of hydraulic parameters. To investigate the bubble rise velocity in chute flows the development of air concentration was analysed to indirectly derive the bubble rise velocity. It was concluded that the bubble rise velocity depends on the amount of local air presence, e.g. 1% or 0.1% air concentration, respectively. It was found that the bubble rise velocity depends on the streamwise Froude number. Air bubbles in high-speed flows typically rise with a velocity of 8 cm/s. Eq. (17) allows to estimate the bubble rise velocity, whereas Eq. (9) gives the bubble size distribution in the uniform flow region. This information may be useful to understand the turbulence effect in high speed flows. Additional data need to be collected in the gradually varied flow region, and in non-prismatic chute reaches with a complex air transport because of the presence of shock waves and three-dimensional flow features.

7. Data CD

All data are available. They are structured on the Data CD into the four chute slopes S_o, the air supply system (aerator or pre-aeration) and the inflow Froude number $\mathbf{F}_o$. The Data CD is available on request at VAW. E-mail: info@vaw.baug.ethz.ch; URL: http://www.vaw.ethz.ch/.

Acknowledgements

This project was supported by the Swiss National Science Foundation, Grant No. 2100-057081.99/1, and the Swiss National Committee on Dams.

References

Boes, R., 2000. Zweiphasenströmung und Energieumsetzung an Grosskaskaden. VAW Mitteilung 166. ETH, Zürich (in German).

Braeske, H., Domnick, J., Brenn, G., 1997. Experimentelle Grundlagenuntersuchungen zur Strömungsmechanik in Blasensäulen. Report LSTM 552/E97. Lehrstuhl für Strömungsmechanik, Technische Fakultät der Friedrich-Alexander-Universität, Erlangen-Nürnberg (in German).

Chanson, H., 1988. Study of air entrainment and aeration devices on spillway models. Report 88-8. University of Canterbury, Christchurch, NZ.

Chanson, H., 1989. Flow downstream of an aerator—Aerator spacing. J. Hydraul. Res. 27, 519–536.

Chanson, H., 1997. Air Bubble Entrainment in Free-Surface Turbulent Shear Flows. Academic Press, London.

Chanson, H., Toombes, L., 2002. Air–water flows down stepped chutes: turbulence and flow structure observations. Int. J. Multiphase Flow 28, 1737–1761.

Comolet, R., 1979. Sur le mouvement d'une bulle de gaz dans un liquide. La Houille Blanche 34, 31–42 (in French).

Falvey, H.T., 1980. Air–water flow in hydraulic structures. Engineering Monograph 41, Bureau of Reclamation, Denver, CO.

Falvey, H.T., 1990. Cavitation in chutes and spillways. Engineering Monograph 42, Bureau of Reclamation, Denver, CO.

Falvey, H.T., Ervine, D.A., 1988. Aeration in jets and high velocity flows. In: Model-Prototype Correlation of Hydraulic Structures, Colorado Springs, Colorado, pp. 25–55.

Haberman, W.L., Morton, R.K., 1956. An experimental study of bubbles moving in liquids. Trans. ASCE 121, 227–252.

Hinze, J.O., 1975. Turbulence. McGraw-Hill, New York.

Kobus, H., 1991. Introduction to air–water flows. In: Wood, I.R. (Ed.), IAHR Hydraulic Structures Design Manual 4, Air Entrainment in Free-Surface Flows. Balkema, Rotterdam, pp. 1–28.

Kramer, K., 2003. Bottom air concentration of aerated chutes. In: 30 IAHR Congress, Thessaloniki, J.F. Kennedy Student Paper Competition, pp. 17–24.

Kramer, K., 2004. Development of aerated chute flow. Ph.D. thesis 15428, ETH, Zurich. Available from: <http://e-collection.ethbib.ethz.ch/show?type=diss&nr=15428>.

Kramer, K., Hager, W.H., Minor, H.-E., 2002. Air detrainment in high-speed chute flows. In: Hydraulic Measurement & Experimental Methods, Estes Park, Colorado: CD-Rom.

Möller, G., 2003. Wasser—Luftgemisch an einer Hochwasserentlastungsanlage. Diploma Thesis, VAW, ETH, Zürich (in German, unpublished).

Rouse, H., 1950. Engineering Hydraulics. John Wiley & Sons, New York.

Rutschmann, P., Volkart, P., Wood, I.R., 1986. Air entrainment at spillway aerators. In: 9 Australasian Fluid Mechanics Conference, Auckland, pp. 350–353.

Schlichting, H., Gersten, K., 1996. Grenzschicht-Theorie. Springer, Berlin (in German).

Soo, S.L., 1967. Fluid Dynamics of Multiphase Systems. Blaisdell Publishing Company, Massachusetts.

Volkart, P., 1985. Transition from aerated supercritical to subcritical flow and associated bubble de-aeration. In: 21 IAHR Congress, Melbourne 5, pp. 2–6.

Wood, I.R., 1988. Aerators—the interaction of nappe and duct air entrainment. In: International Symposium on Hydraulics for High Dams, Beijing, pp. 611–618.